Corrosion Science xxx (xxxx) xxx–xxx

Contents lists available at ScienceDirect

Corrosion Science

journal homepage: www.elsevier.com/locate/corsci

The mechanisms of hot salt stress corrosion cracking in titanium alloy Ti-6Al-2Sn-4Zr-6Mo

Sudha Joseph[a,*], Trevor C. Lindley[a], David Dye[a], Edward A. Saunders[b]

[a] Department of Materials, Royal School of Mines, Imperial College London, Prince Consort Road, London SW7 2BP, UK
[b] Rolls-Royce plc., Materials – Failure Investigation, Bristol BS34 7QE, UK

ARTICLE INFO

Keywords:
Titanium
STEM
X-ray diffraction
Hot corrosion
Hydrogen embrittlement
Stress corrosion

ABSTRACT

Hot salt stress corrosion cracking in Ti 6246 alloy has been investigated to elucidate the chemical mechanisms that occur. Cracking was found to initiate beneath salt particles in the presence of oxidation. The observed transgranular fracture was suspected to be due to hydrogen charging; XRD and high-resolution transmission electron microscopy detected the presence of hydrides that were precipitated on cooling. SEM-EDS showed oxygen enrichment near salt particles, alongside chlorine and sodium. Aluminium and zirconium were also involved in the oxidation reactions. The role of intermediate corrosion products such as Na_2TiO_3, Al_2O_3, ZrO_2, $TiCl_2$ and TiH are discussed.

1. Introduction

Titanium alloys have good corrosion resistance in most circumstances, which makes them attractive in a variety of applications in aerospace and chemical industries [1]. However, these alloys are susceptible to hot salt stress corrosion cracking (HSSCC) when exposed to halides in the temperature range 200–500 °C [2–7]. HSSCC was first reported in Ti-6Al-4V alloy that was creep tested at 370 °C [8]. It has been recently shown that fatigue cracking developed from hot salt stress corrosion is characterised with a distinctive blue spot in low cycle fatigued Ti 6246 alloy [9,10]. Similar HSSCC has also been observed in hot cyclic fatigue spin tests carried out on rotating Ti 6246 gas turbine components [11]. HSSCC in titanium alloys occurs as a two- stage process: crack initiation driven by surface chemistry, followed by crack propagation dependent upon the corrosion kinetics, fracture mechanics and material properties. In general, it is believed that atomic hydrogen produced during the electrochemical reaction between titanium and salt at elevated temperatures is actually responsible for the failure [2,7,12–14]. However, the mechanism by which hydrogen embrittles titanium alloys at high temperatures is not yet fully understood. Hydrogen embrittlement has been suggested to occur by hydrogen decohesion [15], hydrogen enhanced localized plasticity (HELP) [9,10,16,17] and/or brittle titanium hydride formation [7]. In addition to HELP, Absorption Induced Dislocation Emission (AIDE) has recently been observed by Cao et al. during aqueous stress corrosion cracking in α + β titanium alloy[18].

This kind of hot salt stress corrosion failure is mainly observed in laboratory samples and not in aircraft components even though the aircraft environment can often be contaminated by halides. This could be because the airflow in flight might remove corrosion products, preventing the reactions leading to embrittlement. Alternatively, it has been suggested [9,11] that at high pressures (e.g. in a compressor) an oxidation reaction is favoured over the low pressure hydrolysis reaction with moisture [8,12], suppressing hydrogen charging and the corresponding drop in fracture toughness. Therefore the reactions occurring at high pressures will be different from those at low pressures in the laboratory [1,19]. It has been reported that numerous reactions are possible in titanium alloys and number of models have been proposed by various authors to describe the mechanisms of failure [3,20,21].

The main concern of the present work is to investigate the various corrosion products formed during testing, and thereby understand the chemical reactions responsible for failure. In previous work the intermediate corrosion products have not been observed directly; confirmation of the reaction sequence is desirable, as it will improve confidence that these are correctly understood, allowing the integrity of service condition to be established. In this study the jet engine compressor disc alloy Ti-6Al-2Sn-4Zr-6Mo is examined using detailed conventional and analytical TEM in order to make such observations of the reaction sequence.

2. Material and experimental procedure

Rectilinear 60 × 3.5 × 1.5 mm samples were removed from a Ti 6246 forging that was received in a representative condition, Fig. 1a. A

* Corresponding author.
E-mail address: sudha.joseph@imperial.ac.uk (S. Joseph).

https://doi.org/10.1016/j.corsci.2018.02.025
Received 13 July 2017; Received in revised form 14 February 2018; Accepted 16 February 2018

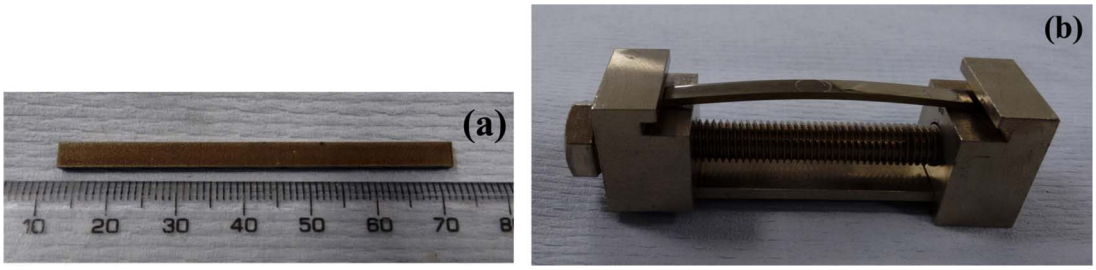

Fig. 1. (a) Ti 6246 alloy sample used for HSSCC testing and (b) 2-point bend rig with a loaded sample.

Table 1
Bend test samples (surface stress applied = 520 MPa) examined in the present study. *The 250 h sample was run on to 350 h.

T(°C)	Duration (hours)			
350	24	60	250*	350
450	24	60		

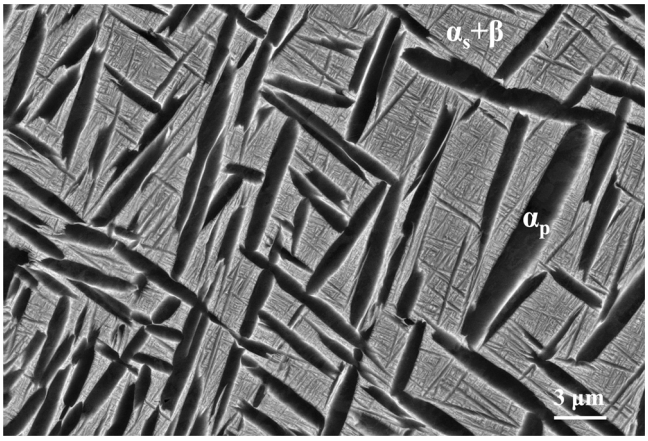

Fig. 2. BSE image showing the typical microstructure of Ti 6246 alloy comprising primary α and secondary α within a retained β matrix.

2-point bend rig [22] was used for loading the sample within a furnace, Fig. 1b. Tests were carried out at 350 and 450 °C for different durations under a surface stress of 520 MPa, below the yield point of the alloy. The test matrix is shown in Table 1. The samples were polished and a droplet of NaCl salt solution (0.1 g of NaCl in 100 ml deionized water) was applied at the center of each sample and allowed to dry before loading the sample in the bend rig. The required stress was achieved by adjusting the holder span of the rig, H

$$H = \frac{KtE(T)\sin\left(\frac{L\sigma}{KtE(T)}\right)}{\sigma} \quad (1)$$

where H is the distance between the two ends of the holder to achieve the desired stress σ, L and t are the length and thickness of the specimen, E (T) is the Young's modulus of the alloy at temperature T, and K is an empirical constant equal to 1.28. The true thickness of the sample was measured prior to loading, after polishing. Both the dimensions of the sample and H were measured using a calibrated digital vernier caliper with an accuracy of ± 0.1 mm. At the test temperatures considered here, a stress drop of approximately 5 MPa is expected due to differential thermal expansion of the steel rig with respect to the sample.

Phase identification of the corrosion products on the sample surface were carried out using a Bruker X-ray diffractometer (D2 Phaser) with Cu Kα radiation of wavelength 1.54 Å. A Zeiss Auriga field emission gun scanning electron microscope (FEG-SEM) in secondary electron (SE) imaging mode was used for metallography and fractography. Electron backscattered (BSE) imaging was used for phase analysis. The chemical compositions of the corrosion products near to the salt particles were measured using energy dispersive X-ray spectroscopy (EDS). For this analysis, an accelerating voltage of 10 kV and a 60 µm aperture were used throughout. To view the corrosion products beneath the salt particles, a cross section of the sample was made in the same SEM by Ga^+ focused ion beam milling.

Transmission electron microscopy (TEM) and scanning TEM (STEM) analysis of the corrosion products were carried out on a failed sample using a JEOL JEM-2100F TEM/STEM operated at 200 kV. The microscope was equipped with an Oxford Instruments X-Max 80 mm^2 silicon drift detector for chemical analysis. The TEM samples for this analysis were prepared using the focused ion beam (FIB) lift-out technique in a dual beam FEI Helios NanoLab 600 using a 30 kV Ga^+ ion beam. TEM foils were lifted out from both the top surface and fracture surface of the failed specimen. To protect the area of interest, a gas injection system was used to deposit a platinum-containing protective layer. Samples were then made electron transparent by thinning down to a thickness of 150 nm. EDS chemical analysis was carried out in STEM mode using a 1 nm probe.

3. Results

3.1. Microstructure

The alloy was β forged, solution treated in α + β phase field, fan air cooled from just below the β transus and then aged at 600 °C. This process gives coarse primary α (α_p) and fine scale secondary α (α_s) in β. The BSE image in Fig. 2 shows the coarse and elongated α_p as well as much finer α_s laths residing within a retained β phase matrix.

3.2. Corrosion test results

3.2.1. Observations on the 350 °C test

Tests were carried out for 24, 60 and 350 h. The 24 h exposure did not show any oxidation near to the salt particles, Fig. 3a. The 60 h exposure was found to have a blue coloration, Fig. 3b, and corrosion deposits around the salt particles, Fig. 3c. Only a few of the many salt particles were observed to have corrosion products nearby and these were only in small quantities. Oxidation was found to increase with time. In this context, oxidation is taken to indicate the formation of oxide corrosion products by pyro-hydrolysis in the presence of salt at elevated temperatures. The 350 h sample was periodically examined during testing and no cracks were observed up to 250 h. A single crack was observed after a long exposure of 350 h, which initiated from a salt particle where significant oxidation had occurred, Fig. 3d. The incubation period for crack initiation at this temperature was therefore between 250 and 350 h.

3.2.2. Observations on the 450 °C test

Significant blue coloration, Fig. 4a, and oxidation near salt particles were observed after 24 h of exposure. But no cracks observed. The sample failed after 60 h exposure. The cracks were initiated beneath salt particles where oxidation had occurred, Fig. 4b and the sample failed by the coalescence of cracks, Fig. 4c and d.